Cooperative Dual-Activity Targeted Nanomedicine for Specific and Effective Prostate Cancer Therapy

Hung-Wei Yang,[†] Mu-Yi Hua,[†,*] Hao-Li Liu,[§] Rung-Ywan Tsai,[‡] Cheng-Keng Chuang,[#,∥] Po-Chun Chu,[§] Pei-Yi Wu,[∥] Ying-Hsu Chang,[∥] Heng-Chang Chuang,[∥] Kai-Jie Yu,[∥] and See-Tong Pang[#,∥,*]

[†]Chang Gung Molecular Medicine Research Center, Department of Chemical and Materials Engineering, Chang Gung University, Kuei-Shan, Tao-Yuan 33302, Taiwan R.O.C., [§]Department of Electrical Engineering, Chang-Gung University, Kuei-Shan, Tao-Yuan 33302, Taiwan R.O.C., [‡]Electronics and Optoelectronics Research Laboratories, Industrial Technology Research Institute, Hsinchu 31040, Taiwan R.O.C., [#]Graduate Institute of Clinical Medical Sciences, Chang Gung University, 259 Wen-Hwa first Road, Kuei-Shan, Tao-Yuan 33302, Taiwan R.O.C., and [∥]Department of Urology, Chang Gung Memorial Hospital, Tao-Yuan 33305, Taiwan R.O.C. H. W. Yang, M. Y. Hua, and H. L. Liu contributed equally to this work.

ABSTRACT A key issue in cancer therapy is how to enhance the tumor-targeting efficacy of chemotherapeutic agents. In this study, we developed a cooperative dual-targeted delivery platform for paclitaxel (PTX) that has potential application as a powerful prostate cancer treatment. The nanomedicine was prepared by first conjugating PTX to nontoxic high-magnetization nanocarriers which can be actively guided and targeted by an external magnet. Next, the surface was functionalized with carboxylated *o*-(2-aminoethyl)polyethyleneglycol (NH_2-EPEG-COOH) to enable uptake by the reticuloendothelial system. Antiprostate-specific membrane antigen antibodies (APSMAs) were then conjugated onto the carrier to recognize the extracellular domain of the prostate-cancer specific membrane antigen (PSMA), thus binding to cancer cells as a secondary active targeting mechanism. We found a significant enhancement of PTX concentration at the tumor site by nearly 20-fold. In addition, the drug half-life was prolonged more than 4.1-fold (from 24 to 99 h) at 37 °C. Low-dose (4.5 mg/kg) injection of the dual-targeted therapeutic nanomedicine in the presence of magnetic targeting significantly prolonged the median survival of nude mice from 35 to 58 days compared to mice that received a high dose (6 mg/kg) of free PTX. This report demonstrates the potential utility of targeted nanomedicine in the clinical treatment of cancer.

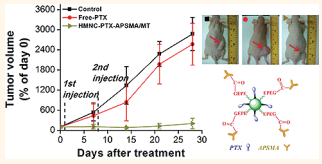

KEYWORDS: dual-targeted nanomedicine · PSMA · anti-PSMA · magnetic targeting · prostate cancer therapy

Prostate cancer (PCa) is the most frequently diagnosed cancer and the second leading cause of death in men in the USA.[1] Of all cancers, the incidence of prostate carcinoma increases the most rapidly with age.[2] Both the prostate gland and PCa are dependent on androgens for growth; their withdrawal induces active regression of the gland *via* epithelial cell apoptosis,[3−5] and a similar phenomenon in PCa cells. For advanced PCa, endocrine therapy by androgen ablation remains the mainstay of treatment. However, as the disease progresses, eventual hormone-resistance of the cells usually results in death.

After endocrine therapy, chemotherapy with drugs such as paclitaxel (PTX) and docetaxel is the primary clinical treatment to prolong the progression-free period and overall patient survival.[6] However, chemotherapeutics induce serious toxicity in other healthy organs and especially in the hematologic system. In addition, therapeutic efficacy is limited by poor penetration of drugs into tumor tissues, only three to five cell diameters from the blood vessels.[7,8] Efficacy can be increased by targeting specific sites in the body. Either molecular targeting using specific peptides or antibodies,[9−16] or magnetic targeting using magnetic drug nanocarriers[17−21] results in high concentrations of drug deposition at the target site while minimizing nonspecific toxicity.[22]

One promising candidate for targeted PCa therapy is prostate-specific membrane antigen (PSMA), a 100-kDa type II glycosylated transmembrane protein that is specifically overexpressed on the surface of human PCa cell lines (LNCaP and CWR22R). PSMA participates in membrane recycling and becomes internalized through ligand-induced endocytosis.[23,24] Low binding and uptake of drugs have been detected in PC3 prostate carcinoma cells, which do not express significant levels of PSMA.[25,26]

Although there have been several reports of targeting nanomedicine to tumor cells using specific biomolecules,[9−16] the delivery efficiency has generally been low because of insufficient target-binding ability or activation of the drug, and short circulation times in the blood. These studies

* Address correspondence to huamy@mail.cgu.edu.tw (M.-Y. Hua), pst64lab@gmail.com (S.-T. Pang).

Received for review December 12, 2011 and accepted January 16, 2012.

Published online January 16, 2012
10.1021/nn2048526

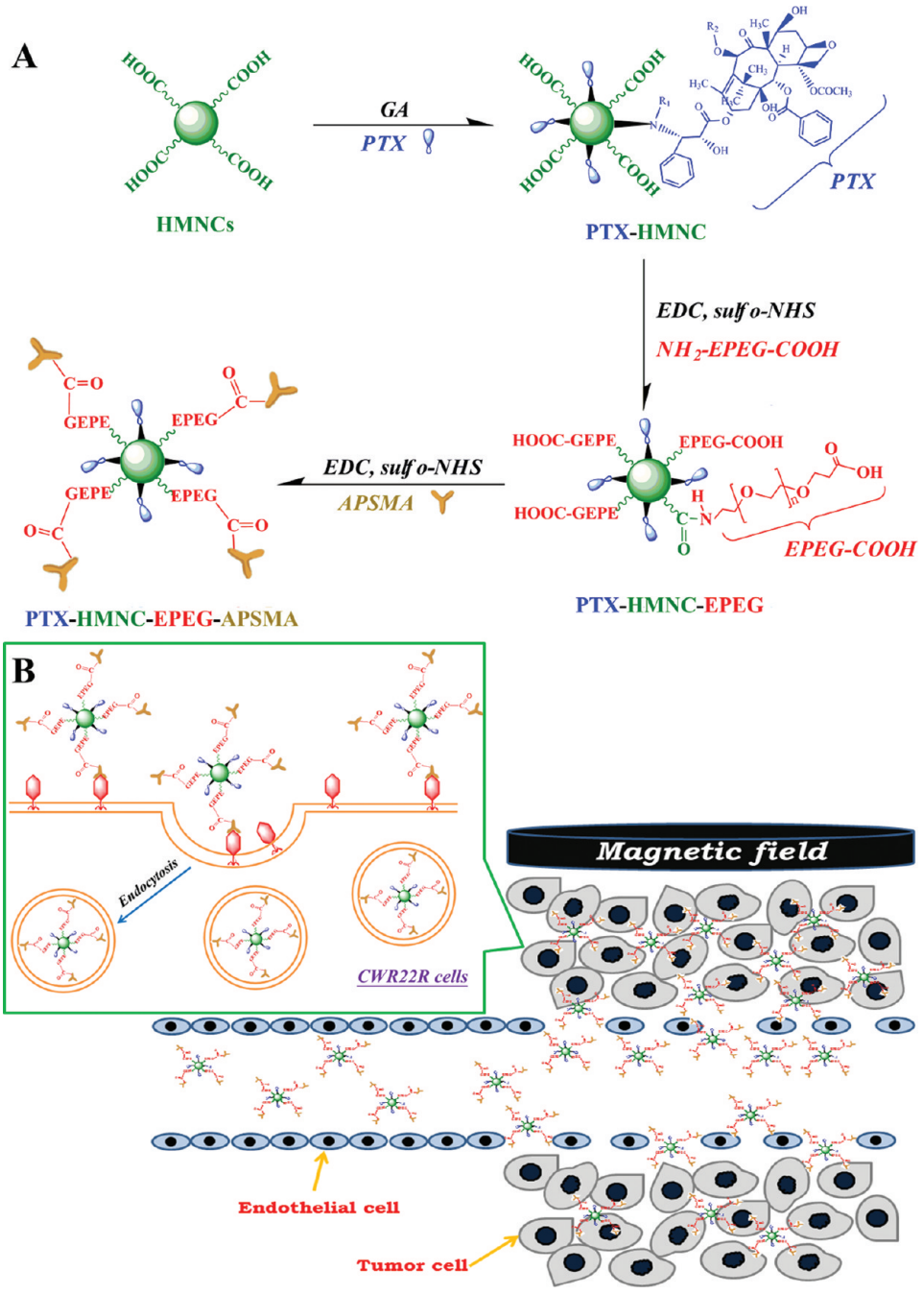

Figure 1. (A) Stepwise synthesis of the smart nanomedicine, PTX-HMNC-EPEG-APSMA. (B) The mechanism of action of PTX-HMNC-EPEG-APSMA for targeted cancer chemotherapy in a magnetic field.

suggest that another force such as external magnetic guidance must be applied to assist molecular targeting and to amplify the homing of anticancer drugs to tumors. Superparamagnetic nanoparticles (SMNPs) are actively used as magnetic resonance (MR) contrast agents and magnetic field-guided drug delivery carriers in cancer therapy. However, several factors have limited their application, including insufficient stability in aqueous media and marked reticuloendothelial uptake. The circulation time of SMNPs in blood is only on the order of minutes due to their rapid capture and clearance by macrophages, especially in the liver.[27−29] Surface modifications with polyethylene glycol have therefore been used to prolong the circulation time of SMNPs in the blood.[30−32]

In this study, we developed a dual-targeted nanomedicine (PTX-HMNC-EPEG-APSMA) which combines specific molecular targeting and external magnetic targeting into a cooperative delivery system for treating PCa. This nanomedicine improved targeting efficacy and amplified homing of the drug to tumors. In addition, the nanomedicine was capable of simultaneously functioning as a magnetic resonance imaging (MRI) contrast agent to allow both real-time PCa

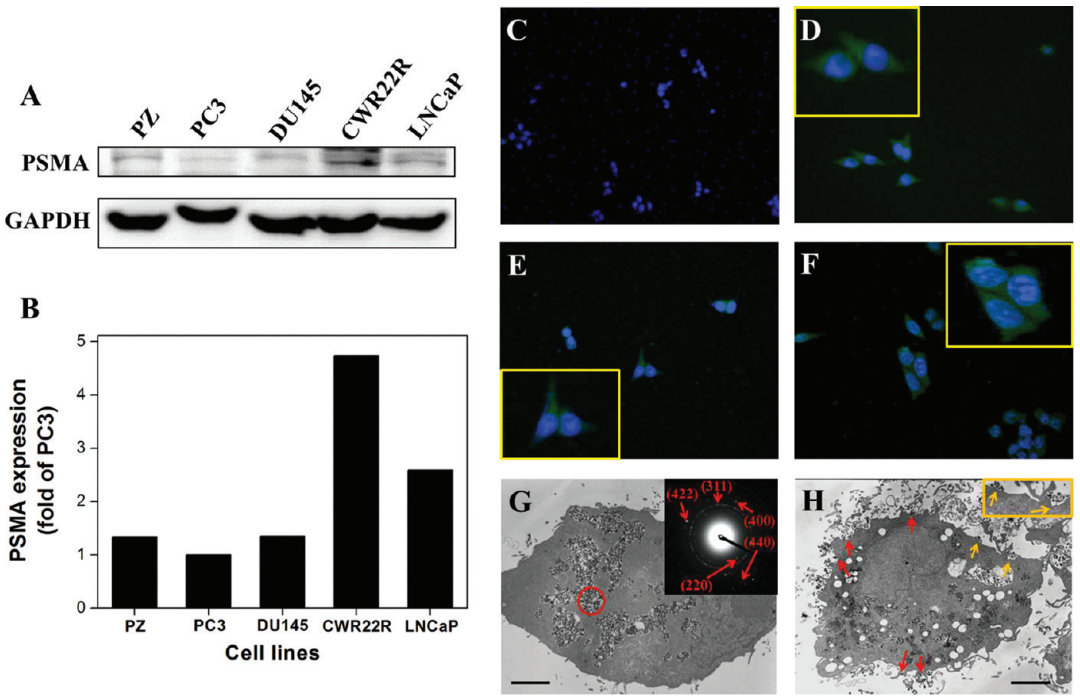

Figure 2. (A) Western blot analysis of PSMA in PCa cells (PC3, PZ, DU145, CWR22R, and LNCaP). (B) Quantification of PSMA expression on the surface of PCa cells. (C–F) Immunofluorescence staining of (C) untreated (control) CWR22R cells or after treatment with (D) free APSMA, (E) HMNC-EPEG-APSMA, or (F) PTX-HMNC-EPEG-APSMA. (G,H) TEM images of CWR22R cells exposed to (G) PTX-HMNC-EPEG and (H) PTX-HMNC-EPEG-APSMA for 4 h (scale bar: 2.6 μm).

imaging and quantification of the targeted drug. Our results provide a promising technological platform for future applications in human cancer chemotherapy.

RESULTS

PTX-HMNC-EPEG-APSMA was synthesized using the described methodology (Figure 1A).[18] It has a high magnetic nanocarrier (HMNC) core and carboxylated EPEG linkers with a mean diameter of approximately 20.3 or 97.6 nm as measured by transmission electron microscopy [TEM] and dynamic light scattering [DLS], respectively. The hydrodynamic size was greater than that measured by TEM, mainly due to the process of sample preparation. The hydrodynamic size was measured in the hydrated state, whereas TEM images depicted the size of dried samples. The nanocarriers were thus expected to have a higher hydrodynamic volume in the hydrated state due to the hydrophilic polymer coating, solvent effect, and concentration effect.[33] The magnetization of the HMNCs was 88.3 emu/g (spin–spin relaxivity = 391.0 mM^{-1} s^{-1}), which decreased to 79.7 emu/g (spin–spin relaxivity = 279.2 mM^{-1} s^{-1}) for PTX-HMNC-EPEG and to 74.4 emu/g (spin–spin relaxivity = 217.9 mM^{-1} s^{-1}) for PTX-HMNC-EPEG-APSMA, likely because of the proportional decrease in Fe_3O_4 per gram of compound. All materials displayed superparamagnetic properties (Supporting Information, Figure S1) with greater magnetization than the commercially available MRI contrast agent, Resovist (73.7 emu/g; spin–spin relaxivity = 103.2 mM^{-1} s^{-1}). Surface functionalization of PTX-HMNC with NH_2-EPEG-COOH and APSMA was carried out under standard amide coupling conditions in the presence of EDC and sulfo-NHS. The FT-IR spectrum of PTX-HMNC-EPEG revealed new peaks that corresponded to PTX and EPEG compared to the spectrum of free HMNC. One peak represented the stretching vibration (ν) of the C–O–C of PTX at 1117 cm^{-1}. The other peaks corresponded to the ν of C=O (1639 cm^{-1}) of the amide group of -NH-EPEG-COOH (conjugated to the carboxyl group of HMNC) and the ν of C–O (1127 cm^{-1}), C–H (2851 and 2926 cm^{-1}), and C=O (1735 cm^{-1}) of the –COOH group of EPEG (Supporting Information, Figure S2). The stretching vibration of Fe–O could still be detected at 584 cm^{-1}. Thus hydrophobic PTX was indeed immobilized on the hydrophilic carriers, and it could be stably suspended in aqueous solutions without any observed precipitation. The surface of PTX-HMNC-EPEG-APSMA has a high negative potential (-40.8 ± 2.4 mV) that prevents severe aggregation[34] and reduces nonspecific interactions between the negatively charged proteins.[35]

High-performance liquid chromatography (HPLC) analysis demonstrated that immobilized PTX reached a saturating concentration of 259.8 μg PTX/mg HMNCs when more than 400 μg of PTX was added (Supporting Information, Figure S3). The maximum concentration of conjugated APSMA was 23.7 μg APSMA/mg PTX- HMNC-EPEG (Supporting Information, Figure S4).

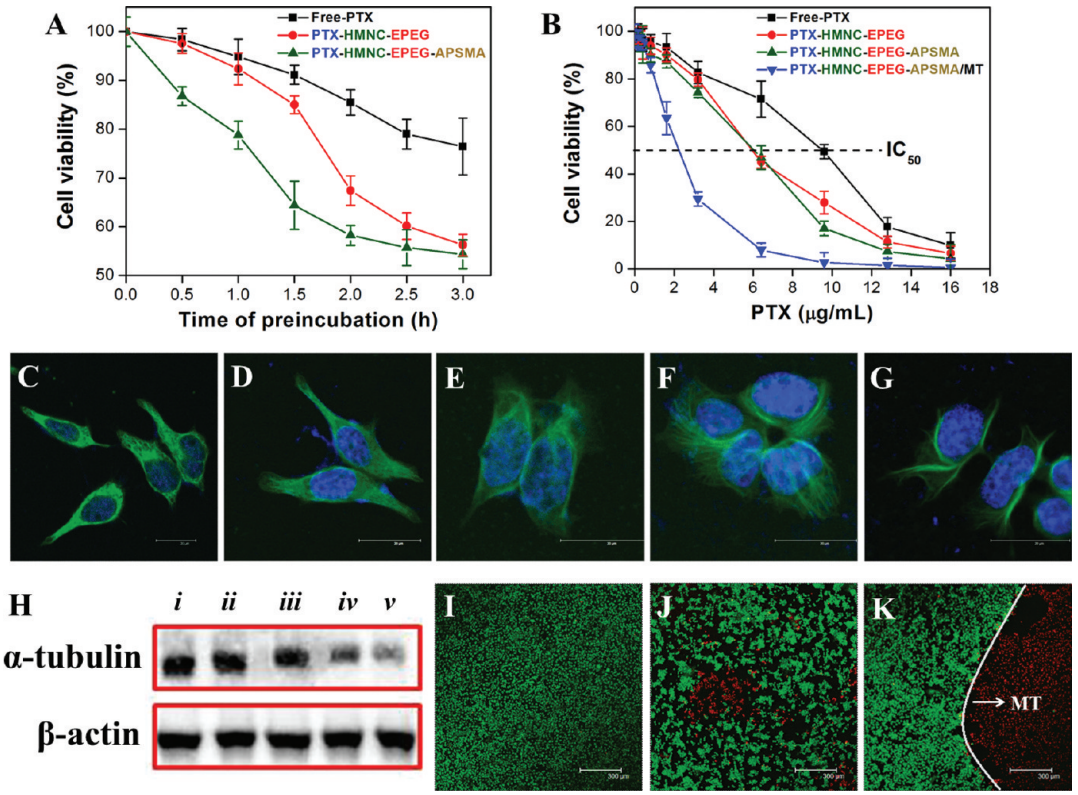

Figure 3. (A) Cytotoxicity of CWR22R cells after pretreatment with free or conjugated PTX for up to 3 h. Values are expressed as means ± SD (n = 8). (B) Cytotoxicity of free and conjugated PTX to CWR22R cells and of PTX-HMNC-EPEG-APSMA with a magnetic field (MT) of 900 gauss, for 24 h. Values are expressed as means ± SD (n = 8). (C−G) Fluorescence micrographs of (C) untreated control CWR22R cells, cells pretreated with (D) free PTX or (E) PTX-HMNC-EPEG-APSMA for 1.5 h, and cells treated with (F) free PTX or (G) PTX-HMNC-EPEG-APSMA/MT for 12 h. (Scale bar, 20 μm; green, α-tubulin; blue, nuclei). (H) Western blot analysis of α-tubulin in CWR22R cells treated with (i) no drug, (ii) free PTX, or (iii) PTX-HMNC-EPEG-APSMA for 1.5 h, or treated for 12 h with (iv) free PTX or (v) PTX-HMNC-EPEG-APSMA and a 900-gauss external magnetic field. (I−K) Fluorescence micrographs of CWR22R cells treated with (I) HMNCs, (J) PTX-HMNC-EPEG-APSMA, or (K) PTX-HMNC-EPEG-APSMA and subjected to a 900-gauss external magnetic field to the right of the white line for 8 h. Green, live cells; red, dead cells (scale bar: 300 μm).

The binding affinity of conjugated APSMA to surface PSMA proteins was up to 64.8%.

The mechanism of PTX-HMNC-EPEG-APSMA action in targeted cancer therapy is presented in Figure 1B. An external magnetic force is first used to guide the nanomedicine from the blood to the tumor site and concentrate it there. The compound then targets PCa cells and enters them by receptor-mediated endocytosis. The activity of conjugated PTX was estimated using a tubulin protein assay.[36] Tubulin assembly by PTX-HMNC-EPEG-APSMA was only 72.7% compared to the same concentration of free PTX, resulting in a maximum effective capacity of 188.9 μg PTX/mg HMNCs (Supporting Information, Figure S5). However, the half-life of PTX stored at 37 °C (Supporting Information, Figure S6) increased from 25 to 61 h after conjugation to HMNC, and to 99 h for PTX-HMNC-EPEG-APSMA. The better thermal stability is expected to prolong the effective circulation time of PTX.

We investigated the expression of PSMA in human PCa cell lines PC3, PZ, DU145, CWR22R, and LNCaP by quantitative Western blot analyses using GAPDH as a loading control and a normalization standard for band intensities (Figure 2A). PSMA was expressed strongly by CWR22R and LNCaP cells and weakly by PC3, PZ, and DU145 cells. Quantitative analysis indicated that the amount of PSMA in CWR22R cells was 1.9-fold higher than in LNCaP cells and 4.7-fold higher than in PC3 cells (Figure 2B). We concluded that CWR22R cells were a suitable PCa model to investigate the accumulation and specificity of molecular targeting with APSMA .

We used immunofluorescence staining to investigate the binding efficacy of APSMA to PSMA on CWR22R cells. After a 1 h exposure of CWR22R cells to free APSMA, a fluorescein isothiocyanate (FITC) signal was clearly visible on the cell surface (Figure 2D) compared to the untreated control (Figure 2C), indicating specific binding of APSMA to the CWR22R PCa cells. CWR22R cells were also specifically targeted by the bioconjugated forms of APSMA, HMNC-EPEG-APSMA (Figure 2E), and PTX-HMNC-EPEG-APSMA (Figure 2F).

TEM images confirmed that PTX-HMNC-EPEG and PTX-HMNC-EPEG-APSMA were both small enough to penetrate tissues and be taken up effectively by tumor cells after 4 h of coculture *via* several endocytic pathways (caveolae-mediated endocytosis, macropinocytosis,

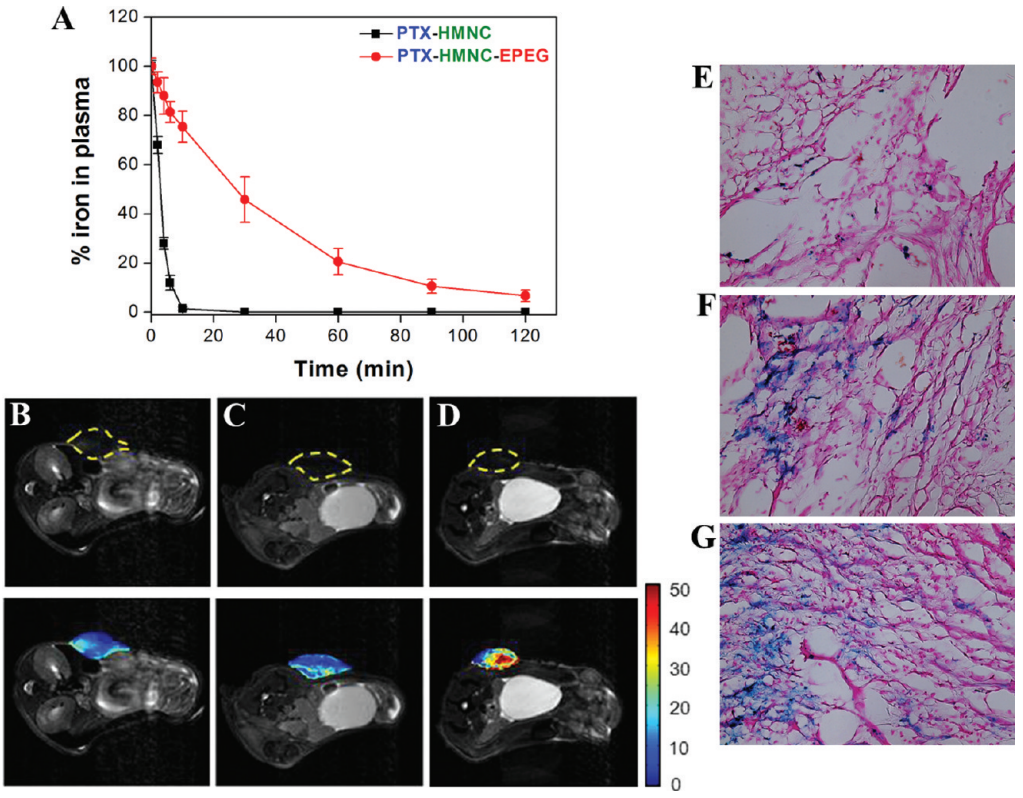

Figure 4. (A) *In vivo* behavior of the untargeted nanomedicine in mice. The percentage of Fe remaining in circulation is expressed as a function of time with an injection dose of 9.8 mg HMNC-EPEG/kg (~391.1 μg/mouse) ($n = 3$). *In vivo* imaging of the distribution of PTX-bioconjugates in hypodermic tumors treated with (B) PTX-HMNC-EPEG, (C) PTX-HMNC-EPEG-APSMA, or (D) PTX-HMNC-EPEG-APSMA with magnetic targeting (0.4 T) for 12 h (top, T2-weighted images; bottom, combined R2 maps and T2-weighted images). Staining with Prussian Blue (100×) revealed the uptake of Fe in tumor tissues after treatment with (E) PTX-HMNC-EPEG-APSMA, (F) PTX-HMNC-EPEG with MT for 12 h, and (G) PTX-HMNC-EPEG-APSMA with MT for 12 h (blue: Fe).

or clathrin-mediated endocytosis, depending on the particle size) (Figure 2G,H).[37] More PTX-HMNC-EPEG-APSMA was attached to the CWR22R cell membranes compared to PTX-HMNC-EPEG, and the APSMA-conjugated drug entered the targeted cancer cells through receptor-mediated endocytosis (Figure 2G,H). Diffraction analysis of a selected area confirmed that the black nanoparticles in the cells were Fe_3O_4 crystals (Figure 2G, inset). These data suggested that our strategy could be used to target PSMA-overexpressing cell lines to enhance the specificity and accumulation of PTX.

To investigate how targeting affected drug delivery, free or conjugated forms of PTX were precultured with cells at 37 °C. Cell viability was 91.1% after treatment with free PTX and 85.1% with PTX-HMNC-EPEG, but decreased significantly to 64.4% after 1.5 h of PTX-HMNC-EPEG-APSMA treatment, indicating that PTX could attach to the cell surface through multivalent interactions between PSMA and APSMA. Cell viability was not significantly different between PTX-HMNC-EPEG and PTX-HMNC-EPEG-APSMA at increased incubation times of 3 h, because PTX-HMNC-EPEG could enter the cells by endocytosis after 2 h of coculture (Figure 3A). All forms of the drug were toxic toward CWR22R cells in a dose-dependent manner (Figure 3B). The IC_{50} (concentration required for 50% inhibition of cellular growth) of free PTX was 9.4 μg/mL, which was higher than that of PTX-HMNC-EPEG and PTX-HMNC-EPEG-APSMA (both 5.9 μg/mL). The IC_{50} of PTX-HMNC-EPEG-APSMA was significantly further reduced to 2.2 μg/mL when a 900-gauss magnetic field was applied, presumably because more PTX-HMNC-EPEG-APSMA was guided to the cells, further enhancing the local drug concentration.

The interaction of PTX-conjugates with tubulins is mediated by the C-2 benzoate, C-2′ hydroxyl, and C-3′ phenyl groups of PTX. PTX-conjugate treatment results in rapid assembly of cellular α-tubulin into microtubules, without disassembly into tubulin subunits, thus reducing the amount of intracellular α-tubulin resulted in the cells not proceeding to mitosis to induce the apoptosis. Immunofluorescence staining with anti-α-tubulin-FITC was used to confirm the anticancer mechanism of PTX. Free PTX preincubated with cells for 1.5 h had no significant effect on the dynamic balance between α-tubulin and microtubules compared to the control (Figure 3C and 3D). In contrast, cytoplasmic α-tubulin levels were reduced after preincubation with PTX-HMNC-EPEG-APSMA for 1.5 h (Figure 3E). Like the cell viability results, these data suggested that PTX was

TABLE 1. The Quantification of Fe and PTX in Tumor Tissues

	Fe (μg/mouse)	PTX (μg/mouse)
free-PTX[a]	—	2.6 ± 1.2
PTX-HMNC[b]	7.8 ± 2.4	2.2 ± 0.7
PTX-HMNC-EPEG[b]	10.6 ± 3.1	3.7 ± 0.9
PTX-HMNC-EPEG-APSMA[b]	19.8 ± 4.6	5.7 ± 1.3
PTX-HMNC-EPEG/MT[b,c]	132.6 ± 16.1	38.4 ± 4.7
PTX-HMNC-EPEG-APSMA/MT[b,c]	178.1 ± 19.7	51.6 ± 5.7

[a] The initial injection doses of PTX was 6.0 mg/kg (~198.1 μg/mouse). [b] The initial injection doses of Fe and PTX were 13.1 mg/kg (~429.1 μg/mouse) and 4.5 mg/kg (~148.5 μg/mouse), respectively. [c] The accumulation was estimated after removing the magnetic field of 6 h.

capable of attaching to the cell surface and entering the cells through receptor-mediated endocytosis before removal of the drug-containing medium. Free PTX efficiently reduced α-tubulin levels after a longer incubation period, confirming the major anticancer mechanism of PTX (Figure 3F). The PTX-HMNC-EPEG-APSMA-dependent reduction in α-tubulin expression was significantly enhanced by application of a magnetic field during the culture period, presumably due to the increased local drug concentration (Figure 3G). The reduction in α-tubulin levels was confirmed by Western blot analyses using β-actin as a control (Figure 3H).

Fluorescence microscopy confirmed that HMNC-EPEG had no cytotoxic effect (Figure 3I), whereas some dead cells (red) appeared with PTX-HMNC-EPEG-APSMA (Figure 3J). The majority of PTX-HMNC-EPEG-APSMA-incubated CWR22R cells died only in the region of the plate that was exposed to a 900-gauss magnetic field (Figure 3K). Taken together, these results suggested that PTX can be concentrated at a targeted site using an external magnetic field to enhance its cytotoxic effects against cancer cells.

A long circulation time in the bloodstream is a key requirement for specific targeting of nanomedicine and *in vivo* drug delivery. PTX-HMNC was modified with functional NH_2-EPEG-COOH to prolong its circulation in the blood. The amount of Fe remaining in systemic circulation 6 min after drug administration was 81% for PTX-HMNC-EPEG and 12% for PTX-HMNC. The blood half-life of PTX-HMNC-EPEG was significantly prolonged to 26.8 min compared to 2.9 min for PTX-HMNC (Figure 4A).

Next we investigated the efficacy of *in vivo* local delivery of PTX-bioconjugates into subcutaneous tumors by molecular and magnetic targeting. MR T2-weighted imaging was used to evaluate the susceptibility to artifact-induced signal loss caused by HMNC accumulation, and spin−spin relaxation (R2) maps were used to detect changes caused by different amounts of HMNCs. We found that a small amount of PTX-HMNC-EPEG had accumulated due to the enhanced permeability and retention (EPR) effect (Figure 4B). Accumulation was slightly increased by the multivalent effect of APSMA binding to PSMA on the cell membrane (Figure 4C). However, accumulation of PTX-HMNC-EPEG-APSMA was significantly increased by approximately 10.3-fold at the tumor site after a 12-h exposure to MT (Figure 4D) compared to no MT treatment (Figure 4C). Inductively coupled plasma optical emission spectrometry (ICP−OES) confirmed the results of MRI R2 maps. The concentration of accumulated Fe was 178.1 μg/mouse after 12 h of MT coupled with injection of PTX-HMNC-EPEG-APSMA, which was higher than injections of PTX-HMNC (7.8 μg/mouse), PTX-HMNC-EPEG (10.6 μg/mouse), PTX-HMNC-EPEG-APSMA alone (19.8 μg/mouse), and PTX-HMNC-EPEG with MT (132.6 μg/mouse) (Table 1). On the basis of our previous studies, we concluded that R2 maps can serve as a good tool not only for quantification but also for imaging the local distribution of magnetic nanomedicines *in vivo*.[19] The significant increase in the deposition of PTX-bioconjugates at the tumor site by MT treatment was histologically confirmed by Prussian blue staining. In addition, the level of PTX-HMNC-EPEG-APSMA/MT accumulation (Figure 4G) was increased compared to that of PTX-HMNC-EPEG/MT (Figure 4F) when the magnetic field was removed for 6 h. This increase occurred because PTX-HMNC-EPEG-APSMA was bound to the cell surface by multivalent forces during the MT period, indicating that a combination of molecular and magnetic targeting could maximize the accumulation of chemotherapeutic drugs (Figure 4E−G).

Treatment efficacy using free PTX and PTX-bioconjugates was evaluated in mice with hypodermic tumors induced by the injection of CWR22R cells (Figure 5A). The combination of PTX-HMNC-EPEG-APSMA and 12 h of MT was most effective for controlling tumor progression. Approximately 34.7% (51.6 ± 5.7 μg) of the initial dose (ID) (148.5 μg/mouse) of PTX was concentrated at the tumor, which was 26.7-fold higher than for free PTX injection (1.3% ID). Over a 28-day period, the tumor volume increased by 202 ± 153% in the PTX-HMNC-EPEG-APSMA/MT-treated group (effective PTX dose of 4.5 mg/kg) and by 888 ± 234% in the PTX-HMNC-EPEG/MT-treated group (effective PTX dose of 4.5 mg/kg) compared to 2873 ± 495% in the untreated control group and 2568 ± 624% for treatment with free PTX (6.0 mg/kg). Tumor growth was slightly inhibited (1952 ± 382%) in the PTX-HMNC-EPEG-APSMA-treated group without MT, indicating that molecular targeting increased binding affinity but was not sufficient to overcome the effects of blood flow and uptake by macrophages. In contrast, magnetic targeting played an important role in enhancing the accumulation of PTX-bioconjugates at the tumor site. Although the conjugates could escape from the tumor tissue *via* the bloodstream after removal of the

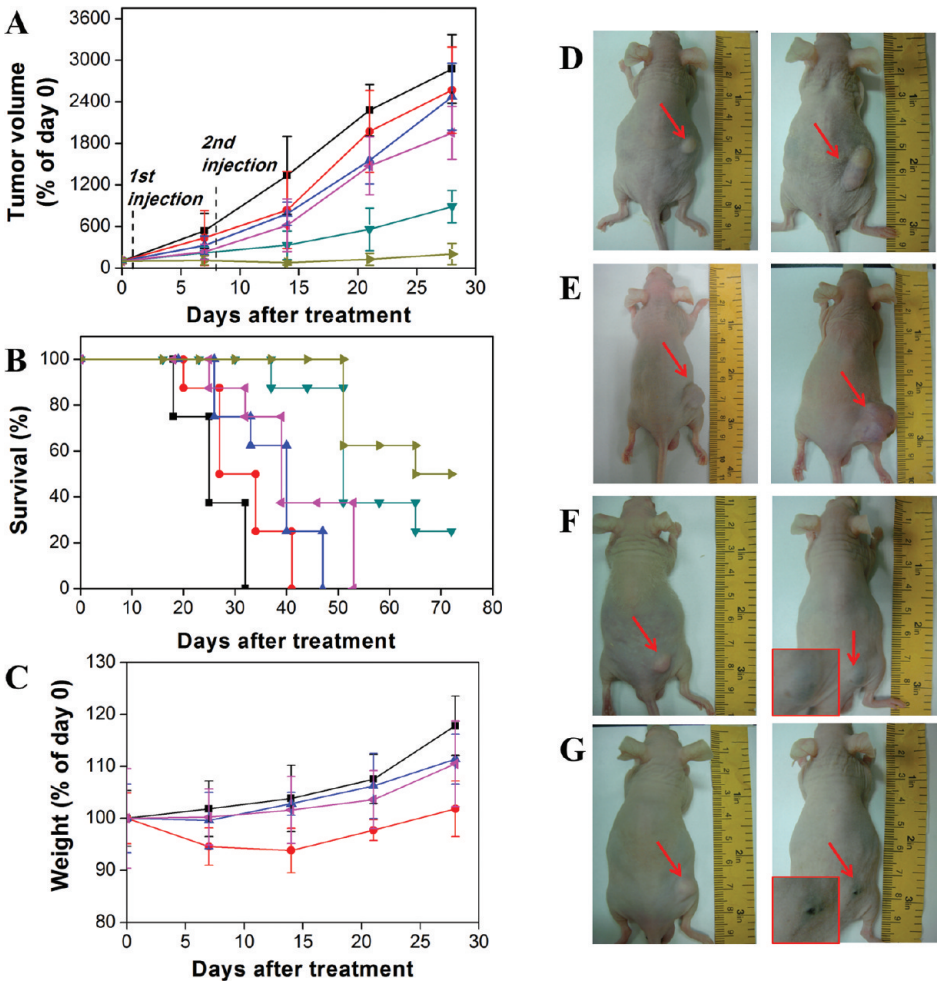

Figure 5. (A) Quantitative analysis of the effects of various treatments on tumor size. Values are means ± SD (n = 8). (B) Survival plots of animal experiments. PTX-HMNC-EPEG-APSMA combined with MT provided the most significant suppression of tumor progression and increase in animal survival relative to the other groups. Values are represented as means ± SD (n = 8). Animals were euthanized when the implanted tumor volume reached 3 cm^3. (C) Total body weight changes after intravenous treatment in the subcutaneous mouse model of PCa. Values are means ± SD (n = 8): (black square) control; (red dot) free PTX; (blue triangle) PTX-HMNC-EPEG; (green triangle) PTX-HMNC-EPEG/MT; (pink triangle) HMNC-EPEG-APSMA; (brown triangle) PTX-HMNC-EPEG-APSMA/MT). (D–G) Images of representative mice at the initial point (before treatment, left) and the end point (28 days after treatment, right) for (D) control, (E) free PTX, (F) PTX-HMNC-EPEG/MT, and (G) PTX-HMNC-EPEG-APSMA/MT groups. Images were obtained over a 28-day period. The scar tissue and underlying skin at the injection site are shown for the PTX-HMNC-EPEG-APSMA/MT group, which achieved complete tumor regression. Red arrows indicate the position of the implanted tumor.

external magnetic field, PTX-HMNC-EPEG-APSMA became bound to PSMA expressed on the surfaces of the CWR22R cells, maintaining the high concentration of the drug and resulting in a 1.3-fold higher amount of Fe than in the PTX-HMNC-EPEG/MT-treated group (Table 1). This delivery method may thus provide a more specific and effective inhibition of tumor growth at lower drug doses, which would reduce the side effects of chemotherapy. Treatment with HMNC-EPEG alone or with HMNC-EPEG/MT was ineffective for inhibition of tumor growth, indicating that the accumulation of HMNC-EPEG at the tumor site did not obstruct the blood vessels and would therefore not be expected to induce necrosis of the tumor tissue, consistent with our previous results.[21]

Although treatment with free PTX or PTX-HMNC-EPEG-APSMA alone increased median animal survival from 25 days to 35 and 39 days, respectively, the survival increased significantly (more than 72 days) in animals receiving PTX-HMNC-EPEG or PTX-HMNC-EPEG-APSMA together with 12 h of MT treatment (median survival: 51 days for PTX-HMNC-EPEG/MT and 65 days for PTX-HMNC-EPEG-APSMA/MT; Figure 5B). Only the mice receiving 6 mg/kg of free PTX exhibited a slight weight loss, whereas those receiving the PTX-bioconjugates did not lose weight during the 28-day treatment period (Figure 5C). Blood biochemistry analyses confirmed that neither liver nor renal functions were affected, even at 14 days after injection of the highest dose of HMNC-EPEG (30 mg/kg) (Figure S7). Photographs of mice confirmed that treatment with

PTX-HMNC-EPEG-APSMA/MT was significantly more effective for tumor reduction compared to controls (Figure 5D–G). Passive tumor targeting of systemic nanomedicine is affected by both particle size and charge, with cationic[38] and smaller[39] particles accumulating to higher levels. Our dual-targeted nanomedicine was designed to have a cationic surface and a small size to facilitate its accumulation within tumors.

DISCUSSION

Several nanoparticle systems for PCa treatment have previously been developed to improve the efficacy of drug delivery and to decrease the incidence of serious side effects. Here we designed a cooperative dual-targeted nanomedicine for increased specific drug accumulation and more effective delivery of PTX to tumors. The potential advantages of our design include the use of strong magnetization (86.1 emu/g) to overcome the magnetic gradient decay with distance,[36,40] a small size (20.3 nm) to avoid thrombosis in blood vessels and organs, functional EPEG to prolong circulation in the bloodstream, and high PSMA binding affinity (64.8%) to increase targeting to tumor cells. In addition, PTX-HMNC-EPEG-APSMA is a better MRI contrast agent than Resovist, both *in vitro* and *in vivo* (217.9 mM^{-1} s^{-1} for HMNCs *vs* 103.2 mM^{-1} s^{-1} for Resovist). Thus, combining dual-targeting and high contrast ability provides improved image resolution and quantitative information on the deposition of anticancer therapeutics.

Effective therapy requires a high efficiency of PTX immobilization on the surface of the carriers. Our bioconjugation method had a superior payload of PTX, and also enhanced its thermal stability. HMNCs offer increased binding sites (carboxylic acid groups) and sufficient space for PTX. The degrees of freedom of the C-2 benzoate group, C-2′ hydroxyl group, and C-3′ phenyl group of PTX are limited after bioconjugation. The resultant decrease in activity of PTX may be caused by weakened interactions of these functional groups with tubulin,[40,41] which drastically reduces the conformational changes of PTX and enhances its thermal stability. The half-life of PTX was found to be longer due to protection by the outer layer of carboxylated EPEG linkers, which drastically reduces PTX distortion and prevents contact with the surrounding medium.[21] This improvement maintains the cytocidal activity of PTX, which involves interacting with tubulin proteins to destroy the cytoskeletal system.

The specific cancer cell surface antigen PSMA is expressed at 1000-fold higher levels in PCa than in the normal epithelium, and its expression levels increase with disease progression.[42] PSMA-specific ligands or antibodies are thus good candidates for PCa targeting and have the potential to increase the accumulation and specificity of chemotherapeutic agents at the tumor site. Long, hydrophilic carboxylated EPEG linkers were incorporated onto the surface of the nanomedicine to reduce opsonization and to prolong the time in the blood circulation from 6 min to approximately 120 min before removal by the reticuloendothelial system.[43] Although the combination of carboxylated EPEG and APSMA biomodifications enhanced tumor-targeting efficacy of PTX-HMNC-EPEG-APSMA by 4.6% ID compared to other targeted nanoparticle systems,[44,45] the efficacy was still not sufficient to effectively inhibit tumor progression. Effective homing to and penetrating of tumor targets requires a blood half-life of longer than 6 h, and modification of the nanomedicine surface with targeting ligands or antibodies that contain charged domains will generally be recognized by macrophages, resulting in drug elimination.[43] To overcome the short half-life, we introduced an external magnetic force to guide and concentrate PTX-HMNC-EPEG-APSMA in the tumor tissue, resulting in significantly improved tumor-targeting efficacy (41.5% ID) compared to magnetic targeting of PTX-HMNC-EPEG (30.9% ID), as well as a reduction in the drug burden on the liver. This difference is likely due to the escape of accumulated PTX-HMNC-EPEG *via* the bloodstream after removal of the external magnetic force. The accumulated nanomedicine can easily pass into and out of tumor vessels because of incomplete tumor vasculature, which is characterized by leaky vessels with gap sizes of 100 nm to 2 μm.[46] Thus, the significant enhancement of tumor-targeting by the magnetic field can be further increased by the specific bioconjugate APSMA which maintains drug accumulation within tumor tissues.

We used a mouse model to show that cooperative and synergistic therapy with dual-targeting nanomedicine could significantly concentrate PTX in the blood vessels at the tumor site to allow entry into the tumor tissue through the EPR effect, which reduced the required drug dose, mitigated toxic side effects, and more effectively inhibited prostate cancer. The high tumor-targeting efficacy of PTX-HMNC-EPEG-APSMA resulted in a significant inhibition of tumor growth after 28 days of treatment and a prolonged median survival (65 days vs 25 days in the control group). Tumors likely recurred due to rapid propagation of any remaining unkilled cancer cells in the absence of further injections after 28 days of treatment. Thus, increasing the number of injections may be expected to cure tumors. In short, we have shown here that treatment with PTX-HMNC-EPEG-APSMA/MT was significantly more effective for tumor reduction with a low dose and just two injections compared to untreated and free-PTX treated control mice. These effects were attributed to maintenance of PTX-HMNC-EPEG-APSMA at a significantly higher concentration in the tumor, while PTX-HMNC-EPEG diffused away over time in the

absence of cellular uptake. Blood biochemical assays performed to investigate the toxicity of HMNC-EPEG revealed that neither liver nor renal functions were affected 14 days after the injection of even the highest dose (30 mg/kg), which indicated that HMNC-EPEG is metabolically eliminated from the liver.

CONCLUSIONS

Here we presented a cooperative dual-targeted nanomedicine that combines molecular and magnetic targeting to increase the local accumulation of an anticancer drug in tumors and enhance its *in vitro* and *in vivo* efficacy against PCa cells. This strategy also significantly prolonged the half-life of PTX to maintain a more effective dose of the drug in the circulatory system. Our findings using a CWR22R mouse xenograft model of PCa suggest that dual-targeted nanomedicine is more effective in reducing prostate tumors at a significantly lower PTX dose. Thus, this study demonstrates an efficient, nontoxic, and specific system for the administration of HMNC-based chemotherapy with significant potential for treating human prostatic carcinoma *in vivo*. Our results form the basis for further development of nanomedical systems to evaluate the most promising candidates for human prostate cancer chemotherapy.

METHODS

Dual-Targeted Nanomedicine Formulation. Briefly, a 0.2-mL aliquot of glutaraldehyde solution (20 wt %) was mixed with 0.2 mL of HMNCs (10 mg/mL) at 25 °C and sonicated for 60 min in the dark at room temperature. After being washed with deionized (DI) water, HMNCs were sonicated with 0.2 mL of PTX for 0.5 h and shaken for another 2.5 h at 10 °C to form PTX-HMNC. Ethyl-3-(3-dimethylaminopropyl) carbodiimide hydrochloride (EDC, 12 mg) and *N*-hydroxysulfosuccinimide sodium salt (sulfo-NHS, 27 mg) were dissolved in 2 mL of 0.5 M MES buffer (pH 6.3) in the dark. A 0.2-mL aliquot of this solution was mixed with 0.2 mL of PTX-HMNC (10 mg/mL) at 25 °C and incubated for 30 min in the dark. After washing with DI water, PTX-HMNC was vortexed with 0.2 mL of NH_2-EPEG-COOH for 2 h in the dark at 25 °C. The resultant PTX-HMNC-EPEG was mixed with EDC and the sulfo-NHS mixture at 25 °C and incubated for 30 min in the dark. After being magnetically separated and washed with DI water, PTX-HMNC-EPEG was vortexed with APSMA for 2 h in the dark at 15 °C to form PTX-HMNC-EPEG-APSMA.

Immunofluorescence Staining. CWR22R cells were grown to approximately 70% confluency on chambered slides. The medium was removed, and cells were fixed for 5 min in ice-cold methanol and rinsed twice with phosphate-buffered saline (PBS). The cells were permeabilized briefly in 0.1% Triton X-100 in PBS for 10 min and washed twice with PBS. Blocking serum (1% BSA in PBS) was added to the chambers, followed by incubation at room temperature for 30 min before aspiration of the solution. The primary antibodies (pure APSMA, HMNC-EPEG-APSMA, and PTX-HMNC-EPEG-APSMA) were added to the cells followed by incubation at room temperature for 1 h. The cells were washed twice with PBST, followed by the addition of a secondary antibody (FITC-labeled mouse antibody), and incubation at room temperature for 1 h. Cells were washed twice with PBST and incubated with DAPI at room temperature for 5 min. Cells were washed twice with PBST and visualized with a fluorescence microscope.

α-Tubulin Reduction Test by Immunofluorescence Staining. CWR22R cells were grown to approximately 70% confluency on chambered slides. Free PTX and PTX-bioconjugates (10 μL of each) were added to the medium and incubated for another 12 h. The medium was removed, and the cells were fixed for 5 min in ice-cold methanol and rinsed twice with PBS. Cells were briefly permeabilized in 0.1% Triton X-100 in PBS for 10 min and washed twice with PBS. Blocking serum (1% BSA in PBS) was added to the chambers followed by incubation at room temperature for 30 min, then removed by aspiration. Cells were then incubated with anti-α-tubulin-FITC at room temperature for 1 h, washed twice with PBS, and stained with DAPI at room temperature for 5 min. Cells were washed twice with PBS and visualized with a fluorescence microscope.

Animal Preparation. All animal experiments were conducted according to protocols approved by Chang Gung University's Institutional Animal Care and Use Committee, and all mice were raised in a 26 °C room. Forty-eight mice (Nu/Nu, 25−30 g) were tested to confirm the efficacy of the proposed approach. Hypodermic PCas were induced by injection of cultured CWR22R cancer cells (1×10^7 cells/mouse). For ethical reasons, animals were euthanized when the volume of the implanted tumor reached 3 cm^3, which was defined as survival. The tumor volume was calculated as: tumor volume (V) = length × width × width/2.[47]

Histology and Microscopy. A separate set of animals was euthanized 24 h after injection of PTX-HMNC-EPEG, PTX-HMNC-EPEG/MT, or PTX-HMNC-EPEG-APSMA/MT. Slides were stained with Prussian blue (Sigma) to detect Fe deposition. Briefly, hypodermic tumor sections mounted on slides were stained with a 1:1 mixture of 2% potassium ferrocyanide and 2% hydrochloric acid for 30 min at room temperature. The slides were rinsed with DI water, counterstained with Nuclear Fast Red for 5 min, dehydrated, and photographed.

Conflict of Interest: The authors declare no competing financial interest.

Acknowledgment. We thank the National Science Council of the Republic of China, Chang Gung Memorial Hospital, and the Industrial Technology Research Institute for financial support (NSC 100-2221-E-182-005, NSC 99-2221-E-182-068, NSC 98-2221-E-182-045-MY3, CMRPD140041, CMRPD140061, CMRPG391781, CMRPG-391782, NMRPD1A1271 and AF51RQ3000). The authors thank Prof. Yu-Sun Chang, who initiated the nanomagnetic drug project at the Chang Gung Molecular Medicine Research Center of Chang Gung University five years ago. We also thank the Chang Gung Memorial Hospital Microscopy Core Laboratory and Animal Molecular Imaging Center for assistance with TEM, confocal microscopy and MRI. Lastly, we dedicate this manuscript to our deceased good friend Dr. Kun-Lung Chuang, who also participated in and contributed to these results.

Supporting Information Available: Additional figures and material as described in the text. This material is available free of charge *via* the Internet at http://pubs.acs.org.

REFERENCES AND NOTES

1. Gao, X.; Porter, A. T.; Grignon, D. J.; Pontes, J. E.; Honn, K. V. Diagnostic and Prognostic Markers for Human Prostate Cancer. *Prostate* **1997**, *31*, 264–281.
2. Jemal, A.; Murray, T.; Ward, E.; Samuels, A.; Tiwari, R. C.; Ghafoor, A.; Feuer, E. J.; Thun, M. J. Cancer Statistics, 2005. *CA Cancer J. Clin.* **2005**, *55*, 10–30.
3. Quinn, M.; Babb, P. Patterns and Trends in Prostate Cancer Incidence, Survival, Prevalence and Mortality. Part II: Individual Countries. *BJU Int.* **2002**, *90*, 174–184.

4. Nakata, S.; Takahashi, H.; Ohtake, N.; Takei, T.; Yamanaka, H. Trends and Characteristics in Prostate Cancer Mortality in Japan. *Int. J. Urol.* **2000**, *7*, 254–257.
5. Mettlin, C. Recent Developments in the Epidemiology of Prostate Cancer. *Eur. J. Cancer* **1997**, *33*, 340–347.
6. Tannock, I. F.; De, Wit, R.; Berry, W. R.; Horti, J.; Pluzanska, A.; Chi, K. N.; Oudard, S.; Théodore, C.; James, N. D.; Turesson, I.; *et al*. Docetaxel Plus Prednisone or Mitoxantrone Plus Prednisone for Advanced Prostate Cancer. *N. Engl. J. Med.* **2004**, *351*, 1502–1512.
7. Hambley, T. W. Is Anticancer Drug Development Heading in the Right Direction? *Cancer Res* **2009**, *69*, 1259–1262.
8. Sugahara, K. N.; Teesalu, T.; Prakash, Karmali P.; Ramana, Kotamraju V.; Agemy, L.; Greenwald, D. R.; Ruoslahti, E. Coadministration of a Tumor-Penetrating Peptide Enhances the Efficacy of Cancer Drugs. *Science* **2010**, *328*, 1031–1035.
9. Ferrari, M. Cancer Nanotechnology: Opportunities and Challenges. *Nat. Rev. Cancer* **2005**, *5*, 161–171.
10. Davis, M. E.; Chen, Z. G.; Shin, D. M. Nanoparticle Therapeutics: An Emerging Treatment Modality for Cancer. *Nat. Rev. Cancer* **2008**, *7*, 771–782.
11. Azarmi, S.; Roa, W. H.; Löbenberg, R. Targeted Delivery of Nanoparticles for the Treatment of Lung Diseases. *Adv. Drug Delivery Rev.* **2008**, *60*, 863–875.
12. Davis, M. E.; Chen, Z.; Shin, D. M. Nanoparticle Therapeutics: An Emerging Treatment Modality for Cancer. *Nat. Rev. Drug Discovery* **2008**, *7*, 771–782.
13. Min, K.; Jo, H.; Song, K.; Cho, M.; Chun, Y. S.; Jon, S.; Kim, W. J.; Ban, C. Dual-Aptamer-Based Delivery Vehicle of Doxorubicin to Both PSMA (+) and PSMA (−) Prostate Cancers. *Biomaterials* **2011**, *32*, 2124–2132.
14. Sanna, V.; Pintus, G.; Roggio, A. M.; Punzoni, S.; Posadino, A. M.; Arca, A.; Marceddu, S.; Bandiera, P.; Uzzau, S.; Sechi, M. Targeted Biocompatible Nanoparticles for the Delivery of (−)-Epigallocatechin 3-Gallate to Prostate Cancer Cells. *J. Med. Chem.* **2011**, *54*, 1321–1332.
15. Akerman, M. E.; Chan, W. C.; Laakkonen, P.; Bhatia, S. N.; Ruoslahti, E. Nanocrystal Targeting *in Vivo*. *Proc. Natl. Acad. Sci. U.S.A.* **2002**, *99*, 12617–12621.
16. Cai, W.; Shin, D. W.; Chen, K.; Gheysens, O.; Cao, Q.; Wang, S. X.; Gambhir, S. S.; Chen, X. Peptide-Labeled Near-Infrared Quantum Dots for Imaging Tumor Vasculature in Living Subjects. *Nano Lett.* **2006**, *6*, 669–676.
17. Rahimi, M.; Wadajkar, A.; Subramanian, K.; Yousef, M.; Cui, W.; Hsieh, J. T.; Nguyen, K. T. *In Vitro* Evaluation of Novel Polymer-Coated Magnetic Nanoparticles for Controlled Drug Delivery. *Nanomedicine* **2010**, *6*, 672–680.
18. Hua, M. Y.; Yang, H. W.; Chuang, C. K.; Tsai, R. Y.; Chen, W. J.; Chuang, K. L.; Chang, Y. H.; Chuang, H. C.; Pang, S. T. Magnetic-Nanoparticle-Modified Paclitaxel for Targeted Therapy for Prostate Cancer. *Biomaterials* **2010**, *31*, 7735–7763.
19. Liu, H. L.; Hua, M. Y.; Yang, H. W.; Huang, C. Y.; Chu, P. C.; Wu, J. S.; Tseng, I. C.; Wang, J. J.; Yen, T. C.; Chen, P. Y.; *et al*. Magnetic Resonance Monitoring of Focused Ultrasound/Magnetic Nanoparticle Targeting Delivery of Therapeutic Agents to the Brain. *Proc. Natl. Acad. Sci. U.S.A.* **2010**, *107*, 15205–15210.
20. Hua, M. Y.; Liu, H. L.; Yang, H. W.; Chen, P. Y.; Tsai, R. Y.; Huang, C. Y.; Tseng, I. C.; Lyu, L. A.; Ma, C. C.; Tang, H. J.; *et al*. The Effectiveness of a Magnetic-Nanoparticle-Based Delivery System for BCNU in the Treatment of Gliomas. *Biomaterials* **2011**, *32*, 516–527.
21. Yang, H. W.; Hua, M. Y.; Liu, H. L.; Huang, C. Y.; Tsai, R. Y.; Lu, Y. J.; Chen, J. Y.; Tang, H. J.; Hsien, H. Y.; Chang, Y. S.; *et al*. Self-protecting Core−Shell Magnetic Nanoparticles for Targeted, Traceable, Long Half-Life Delivery of BCNU to Gliomas. *Biomaterials* **2011**, *32*, 6523–6532.
22. Kim, J. A. Targeted Therapies for the Treatment of Cancer. *Am. J. Surg.* **2003**, *186*, 264–268.
23. Hattori, Y.; Maitani, Y. Enhanced *In Vitro* DNA Transfection Efficiency by Novel Folate-Linked Nanoparticles in Human Prostate Cancer and Oral Cancer. *J. Controlled Release* **2004**, *97*, 173–183.
24. Ghosh, A.; Heston, W. D. Tumor Target Prostate Specific Membrane Antigen (PSMA) and Its Regulation in Prostate Cancer. *J. Cell Biochem.* **2004**, *91*, 528–539.
25. Farokhzad, O. C.; Jon, S.; Khademhosseini, A.; Tran, T. N.; Lavan, D. A.; Langer, R. Nanoparticle-Aptamer Bioconjugates: A New Approach for Targeting Prostate Cancer Cells. *Cancer Res.* **2004**, *64*, 7668–7672.
26. Farokhzad, O. C.; Khademhosseini, A.; Jon, S.; Hermmann, A.; Cheng, J.; Chin, C.; Kiselyuk, A.; Teply, B.; Eng, G.; Langer, R. Microfluidic System for Studying the Interaction of Nanoparticles and Microparticles with Cells. *Anal. Chem.* **2005**, *77*, 5453–5459.
27. Na, H. B.; Song, I. C.; Hyeon, T. Inorganic Nanoparticles for MRI Contrast Agents. *Adv. Mater.* **2009**, *21*, 2133–2148.
28. Gupta, A. K.; Gupta, M. Synthesis and Surface Engineering of Iron Oxide Nanoparticles for Biomedical Applications. *Biomaterials* **2005**, *26*, 3995–4021.
29. Chertok, B.; David, A. E.; Yang, V. C. Polyethyleneimine-Modified Iron Oxide Nanoparticles for Brain Tumor Drug Delivery Using Magnetic Targeting and Intra-carotid Administration. *Biomaterials* **2010**, *31*, 6317–6324.
30. Jang, J. Y.; Lee, D. Y.; Park, S. J.; Byun, Y. Immune Reactions of Lymphocytes and Macrophages against PEG-Grafted Pancreatic Islets. *Biomaterials* **2004**, *25*, 3663–3669.
31. Govender, T.; Riley, T.; Ehtezazi, T.; Garnett, M. C.; Stolnik, S.; Illum, L.; Davis, S. S. Defining the Drug Incorporation Properties of PLA-PEG Nanoparticles. *Int. J. Pharm.* **2000**, *199*, 95–110.
32. Cole, A. J.; David, A. E.; Wang, J.; Galbán, C. J.; Hill, H. L.; Yang, V. C. Polyethylene Glycol Modified, Cross-Linked Starch-Coated Iron Oxide Nanoparticles for Enhanced Magnetic Tumor Targeting. *Biomaterials* **2011**, *32*, 2183–2193.
33. Liu, C. G.; Desai, K. G. H.; Chen, X. G.; Park, H. J. Linolenic Acid-Modified Chitosan for Formation of Self-Assembled Nanoparticles. *J. Agric. Food Chem.* **2005**, *53*, 437–441.
34. Liao, D. L.; Wu, G. S.; Liao, B. Q. Zeta Potential of Shape-Controlled TiO_2 Nanoparticles with Surfactants. *Colloids Surf. A* **2009**, *348*, 270–275.
35. Farokhzad, O. C.; Cheng, J.; Teply, B. A.; Sherifi, I.; Jon, S.; Kantoff, P. W.; Richie, J. P.; Langer, R. Targeted Nanoparticle-Aptamer Bioconjugates for Cancer Chemotherapy *in Vivo*. *Proc. Natl. Acad. Sci. U.S.A.* **2006**, *103*, 6315–6320.
36. Sharma, S.; Ganesh, T.; Kingston, G. I.; Bane, S. Promotion of Tubulin Assembly by Poorly Soluble Taxol Analogs. *Anal. Biochem.* **2007**, *360*, 56–62.
37. Nam, H. Y.; Kwon, S. M.; Chung, H.; Lee, S. Y.; Kwon, S. H.; Jeon, H.; Kim, Y.; Park, J. H.; Kim, J.; Her, S.; *et al*. Cellular Uptake Mechanism and Intracellular Fate of Hydrophobically Modified Glycol Chitosan Nanoparticles. *J. Controlled Release* **2009**, *135*, 259–267.
38. Campbell, R. B.; Fukumura, D.; Brown, E. B.; Mazzola, L. M.; Izumi, Y.; Jain, R. K.; Torchilin, V. P.; Munn, L. L. Cationic Charge Determines the Distribution of Liposomes between the Vascular and Extravascular Compartments of Tumors. *Cancer Res.* **2002**, *62*, 6831–6836.
39. Kong, G.; Braun, R. D.; Dewhirst, M. W. Hyperthermia Enables Tumor-Specific Nanoparticle Delivery: Effect of Particle Size. *Cancer Res.* **2000**, *60*, 4440–4445.
40. Guenard, D.; Gueritte-Voegelein, F.; Potier, P. Taxol and Taxotere: Discovery, Chemistry, and Structure-Activity Relationships. *Acc. Chem. Res.* **1993**, *26*, 160–167.
41. Lee, D. G.; Ponvel, K. M.; Kim, M.; Hwang, S.; Ahn, I. S.; Lee, C. H. Immobilization of Lipase on Hydrophobic Nano-Sized Magnetite Particles. *J. Mol. Catal. B Enzym.* **2009**, *57*, 62–66.
42. Slovin, S. F. Targeting Novel Antigens for Prostate Cancer Treatment: Focus on Prostate-Specific Membrane Antigen. *Expert Opin. Ther. Targets* **2005**, *9*, 561–570.
43. Duncan, R. Polymer Conjugates as Anticancer Nanomedicines. *Nat. Rev. Cancer* **2006**, *6*, 688–701.
44. Weissleder, R.; Kelly, K.; Sun, E. Y.; Shtatland, T.; Josephson, L. Cell-Specific Targeting of Nanoparticles by Multivalent Attachment of Small Molecules. *Nat. Biotechnol.* **2005**, *23*, 1418–1423.
45. Gu, F.; Zhang, L.; Teply, B. A.; Mann, N.; Wang, A.; Radovic-Moreno, A. F.; Langer, R.; Farokhzad, O. C. Precise Engineering

of Targeted Nanoparticles by Using Self-Assembled Biointegrated Block Copolymers. *Proc. Natl. Acad. Sci. U.S.A.* **2008**, *105*, 2586–2591.
46. Byrne, J. D.; Betancourt, T.; Brannon-Peppas, L. Active Targeting Schemes for Nanoparticle Systems in Cancer Therapeutics. *Adv. Drug Delivery Rev.* **2008**, *60*, 1615–1626.
47. Karmali, P. P.; Kotamraju, V. R.; Kastantin, M.; Black, M.; Missirlis, D.; Tirrell, M.; Ruoslahti, E. Targeting of Albumin-Embedded Paclitaxel Nanoparticles to Tumors. *Nanomedicine* **2009**, *5*, 73–82.